Zamre Abdul GHANI, Mohammad Abdul HANNAN, Azah MOHAMED

Dept. of Electrical, Electronic & Systems Engineering, Universiti Kebangsaan Malaysia, 43600 Bangi, Selangor, Malaysia

Investigation of Three-Phase Grid-Connected Inverter for Photovoltaic Application

Abstract. *This paper describes the investigation of the grid-connected three-phase inverter for photovoltaic (PV) application. The inverter control system modeling is carried out in MATLAB/SIMULINK environment. With the aids of the proportional-integral controllers, sinusoidal pulse-width modulation (SPWM) control technique and Park transformation, the inverter control system managed to convert PV power to ac power, stabilize the output voltage and current, and feeds the excess power to the utility grid. The control system generates the PWM signals for power devices, the insulated gate bipolar transistors in order to regulate the output voltage and current. In addition, the system is simulated with the PV simulator in order to facilitate the real PV power that to be fed to the input of the inverter. The control system produced 2.48% and 4.64% of output voltage and current total harmonic distortion, respectively. The simulation results such as the ac output voltages and currents, inverter system power flow, and grid disturbances detection signals, proved the effectiveness of the developed control algorithm. For the validation, this model is to be linked to the inverter prototype by utilizing the dSPACE controller.*

Streszczenie. *W artykule badano trójfazowy przekształtnik w zastosowaniu do urządzeń fotowoltaicznych podłączonych do sieci. Układ składa się ze sterownik PI, układu modulacji SPWM i transformacji Parka i umożliwia konwersję napięcia z systemu fotowoltaicznego do sieci ac, stabilizację napięcia i prądu. (**Badania nad trójfazowym przekształtnikiem podłączonym do sieci w zastosowaniu do urządzeń fotowoltaicznych**)*

Keywords: Photovoltaic; three-phase inverter; grid; PI; SPWM
Słowa kluczowe: systemy fotowoltaiczne, przekształtnik, sieć zasilająca

Introduction

Having realized the importance of finding alternative energy resources for the future energy sustainability, photovoltaic (PV) energy has becomes one of the important renewable energy sources [1]. With the aid of electronics power converters mainly the dc (direct current) boost converters and inverters, this kind of energy can be utilized and transported to the electric utility [2]-[4]. However, the inverter efficiency need to be improved further on in order to mitigate the effects of the self-consumption losses, unbalanced load on inverter output voltage, nonlinearity, PV low efficiency and output fluctuation [5], electromagnetic interference and high level of harmonics content [6]-[13]. In addition, it is important that the inverter system acquires the capability to operate with high speed and frequency in generating the pulse-width modulation (PWM) signals [14]. Hence, the inverter controller which plays an important role in the improvement of the abovementioned issues, needs to be enhanced further to uplift the inverter performance in renewable energy applications, especially in PV. Analogue circuit controllers, microcomputers, digital circuit controllers, field programmable gate arrays (FPGAs) and digital signal processors (DSP), e.g. dSPACE, are among the controllers used in the inverter control system [15]-[25].

In this investigation work, the inverter control system algorithm, strategies and modeling are developed and simulated in MATLAB/SIMULINK. Indeed, the results presented in this paper are based on the simulation environment. However, the successfulness of this modelling is very essential in order to convert it to the prototype later on for the result validation. This simulation creates a potential and justification for hardware realization. For this purpose, the dSPACE controller is utilized for the process of inverter prototype linking. It serves as handy process to develop the control algorithm for the inverter development. The main objective of the inverter control system is to generate and stabilized the 50 Hz sinusoidal-shape ac (alternating current) output voltage and frequency. Having achieved that, together with the grid synchronization algorithm, the interconnecting of the inverter to the utility grid is achievable. Detail explanations of the inverter control system algorithm and its strategy have been discussed.

Grid-Connected Inverter System Description

Fig. 1 illustrates the block diagram of the three-phase grid-connected voltage-source inverter (VSI) PV system for the investigation.

As illustrated, this transformer-less PV system consists of the control system, inverter which interfaces the PV and the grid, harmonic filter, and PV power simulator featuring the maximum power point tracking (MPPT) function.

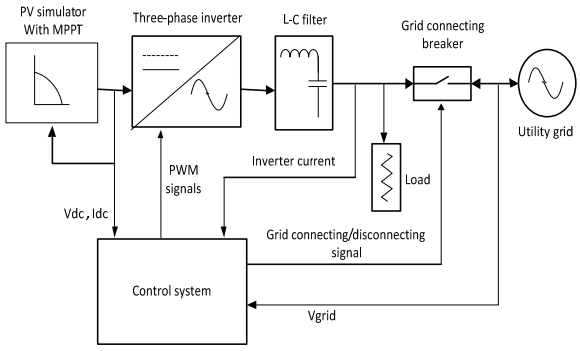

Fig.1. Block diagram of the grid-connected inverter PV system

Firstly the control system consists of several subsystems which include voltage and current control functions, grid synchronization function, PWM generator, abnormal voltage and frequency detection units, e.g. over and under voltage and frequency. For the control algorithm, generating the correct and precise PWM signals for the power devices is the key factor to the generating and regulating the inverter ac output waveforms. By means of the output voltage and current parameters sampling, the system controller is able to transfer the available maximum PV power to the load and simultaneously stabilize the output voltage to a desired level.

Secondly, the PV power simulator with a built-in dc to dc boost converter and maximum power extracting feature, generates and simulates the PV dc power that required for the inverter input stage. With the MPPT algorithm, the system ensures that the maximum power output from the PV is achieved. Basically, different solar irradiations and ambient temperatures exhibit different maximum power output level. For simplification of the analysis, the investigation and simulation are executed only at a fixed solar irradiation of 1000 watt/m^2 and 25º Celsius.

The output voltage of the solar cell is a function of the photocurrent that depends on the solar irradiation level during its operation [26]-[29]. Equation (1) describes the behavior of the output current of the solar cell. The generation of required PV voltage and current for the inverter input stage is achieved by forming the module in series-parallel structure as in equation (2). The power output of the PV array is the product of output current and output voltage of PV represented in equation (3) [30].

$$(1)\quad I_c = I_{ph} - I_o = I_{ph} - I_{sat}\left[e^{\frac{q}{AKT_c}(V+IR_S)} - 1\right]$$

$$(2)\quad V_{PV} = N_s\left[V_{ref} - \beta\left(T - T_{ref}\right) - R_s\left(T - T_{ref}\right)\right]$$

$$I_{PV} = N_P\left[I_{ref} + \alpha\left(\frac{G}{1000}\right)\left(T - T_{ref}\right) + I_{sc}\left(\frac{G}{1000} - 1\right)\right]$$

$$(3)\quad P_{PV} = I_{PV} \times V_{PV}$$

Below are the characteristics of the PV module simulated by the PV simulator during the simulation period:

(i) Open circuit output voltage, V_{oc} = 21.8 V
(ii) Short circuit output current, I_{sc} = 5 A
(iii) Maximum power output voltage, V_{mp}= 17 V
(iv) Maximum power output current, I_{mp} = 4.7 A

In order to produce a total output dc voltage of 408V with a power capacity of 5.8kW, 72 units of PV modules are connected in a series-parallel structure. Then, by utilizing the PV simulator built-in dc to dc boost converter, the voltage is managed to be step-up to 700V to match the inverter input voltage requirement for generating the root-mean-squared (rms) line voltage of 415V. The generated ac voltage and current contain undesired harmonics components which can be reduced or eliminated by the filter. Consequently, the ac output waveform becomes almost sinusoidal in shape. The generated ac power from the inverter is supplied to the load and then dispatched to the grid whenever there is excess power available. The latter case is accomplished through the means of grid-connecting devices, the breaker.

Inverter Control Strategy

The inverter control system operation deals with two modes of operations, standalone and grid-connected. Initially, the system operates in a standalone mode to stabilize the output voltage before gaining the grid synchronization. Once synchronized, the system operates in a grid-connected mode. Fig. 3 illustrates the two-loop control strategy structure for standalone mode, which utilizes PI controllers to regulate the inverter output voltage and the PV input voltage.

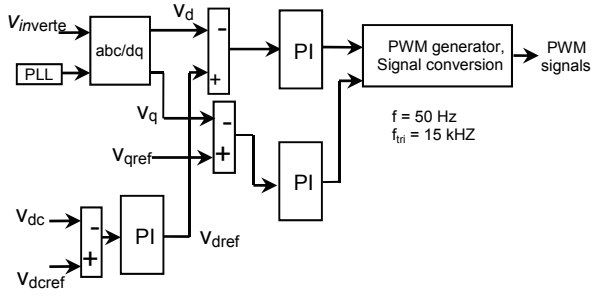

Fig.3. Standalone inverter two-loop voltage control block diagram

The algorithm is made up of several functional blocks such as phase-locked loop (PLL), axes transformation unit (abc/dq frame), voltage regulations, proportional-integral (PI) controllers and PWM signals generation unit.

In standalone mode, the generated power is supplied only to the local loads, without any connection to the grid. In this mode, the inverter operates under voltage-control scheme where the three-phase inverter ac output voltage v_a, v_b and v_c with unity power factor are assumed as in equations (4), are sampled are transformed to dq components. This axes transformation uses the Park transformation [31] and utilizing the 50Hz PLL local or internal synchronizing signal. These voltages are set and arranged so that they are 120° out of phase to each others.

$$(4)\quad \begin{aligned} v_a &= V\sin\omega t \\ v_b &= V\sin(\omega t - \tfrac{2}{3}\pi) \\ v_c &= V\sin(\omega t + \tfrac{2}{3}\pi) \end{aligned}$$

where V is the voltage magnitude and ω is the output frequency. The transformation is governed by the equation (5).

$$(5)\quad \begin{bmatrix} v_d \\ v_q \\ v_o \end{bmatrix} = \frac{2}{3}\begin{bmatrix} \cos\omega t & \cos\left(\omega t - \frac{2\pi}{3}\right) & \cos\left(\omega t + \frac{2\pi}{3}\right) \\ -\sin\omega t & -\sin\left(\omega t - \frac{2\pi}{3}\right) & -\sin\left(\omega t + \frac{2\pi}{3}\right) \\ \frac{1}{2} & \frac{1}{2} & \frac{1}{2} \end{bmatrix}\begin{pmatrix} v_a \\ v_b \\ v_c \end{pmatrix}$$

Under the balanced load condition, the v_o term in the dq coordinate frame can be neglected which left only the v_d and v_q terms. Thus, the PI controllers are able to keep track the reference voltage in both transient and steady-state conditions for error minimization, which stabilizes the inverter output voltages. Then the voltages v_d and v_q are regulated at the reference voltages v_{dref} and v_{qref} respectively by comparing process which generates error voltages. These error voltages are fed to the PI controllers for the output voltage regulation. The time domain PI control algorithm is shown in (6).

$$(6)\quad u(t) = K_p e(t) + K_i \int_0^t e(t)dt$$

where $u(t)$ is the output of the PI controller, K_p and K_i are the controller proportional and integral gains respectively, and $e(t)$ is the generated error signal as in equation (7), i.e. the difference between the reference voltage signal, $r(t)$, and the measured one, $y(t)$.

$$(7)\quad e(t) = r(t) - y(t)$$

The PI controller minimizes the rise time or the overshoot phenomenon and the steady-state error of the inverter output voltage. It calculates the integral of the error and adds it up to the proportionate error. Upon summation, the PI controller generates a control signal in such a way that the error signal is kept to a minimum value [32]. Thus, the system is capable of keeping the output voltage as close as possible to the reference voltage. As a result the inverter output voltage can be controlled and stabilized as desired.

After stabilizing the phase output voltage of 240V_{rms} and frequency of 50Hz, the control system senses the grid voltage, frequency and phase for the grid synchronization. Then the control system starts to establish the grid connection through the grid-connecting breaker and operates in a grid-connected mode. The inverter current is sensed and then transformed to dq components. As shown in Fig. 4, this current control scheme has enables the PI controller to track the reference current based on the error between the actual current components, I_d and I_q, and their reference current, I_{dref} and I_{qref} respectively.

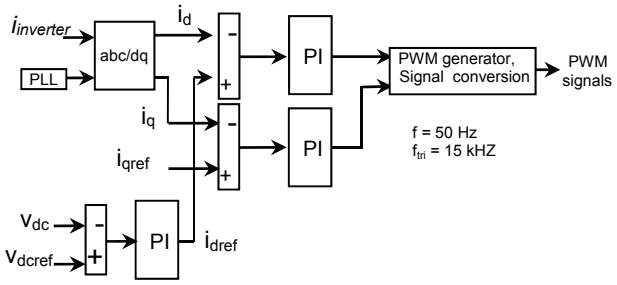

Fig.4. Standalone inverter two-loop current control block diagram

These reference currents are generated from the dc voltage control scheme where the dc link voltage, V_{dc}, is regulated by the PI to track the reference voltage of $700V_{dc}$. For the system protection against the grid disturbances such as frequency and voltage changes, the system implemented the voltage and frequency disturbances detection algorithm. Upon detection of the parameters changes, a cut off signal is send to the breaker to isolate the inverter from the grid, leading to a standalone mode situation.

PWM Signal Generation

At final stage of the two-loop control blocks, the algorithm utilizes the sinusoidal PWM (SPWM) method, where the output of the PI controllers involves in generating the switching signal for the IGBTs. In producing these signals, the control signals which are the modulating signals are compared to the 15 kHz triangular wave. The SPWM is one the method to pulse-width modulate the inverter IGBTs in order to shape the output ac voltages to be as close to a sine wave as possible [33]. The switches duty cycles are modulated by the control signals that is the desired inverter output fundamental frequency. This triangular wave frequency establishes the inverter switching frequency at which the inverter switches are switched [33].

The ac output voltage contains harmonics components which appear as sidebands, centered around the switching frequency and its multiple as in equation (8) [33].

$$f_{harmonic} = k\, M_f\, f_{control} \tag{8}$$

where k is an integer, $f_{control}$ is the frequency of the control signal and M_f is the frequency modulation index as in equation (9).

$$M_f = \frac{f_{triangular}}{f_{control}} \tag{9}$$

The PV input voltage is controlled at a certain voltage reference which resulted in the regulation of ac output voltage as in equation (10)

$$V_{line,rms} = 0.612 M_a V_{dc} \tag{10}$$

where, V_{dc} is the dc input voltage and M_a is the amplitude modulation index. It is the ratio of the amplitude of control signal, $v_{control}$ to the amplitude of triangular wave signal i.e. carrier signal, v_{tri} as shown in equation (11).

$$M_a = \frac{A_{v_{control}}}{A_{v_{tri}}} \tag{11}$$

This parameter determines the value of the inverter fundamental rms output line voltage. It should be maintained in the range of 0.9 so that no over-modulation phenomenon occurs, which resulted of higher output voltage with more harmonics appear in the output waveform and this condition should be avoided.

The outputs of inverter are connected to the electric utility by means of the inductor-capacitor filter without the implementation of an isolation transformer, since it is bulky, heavy and costly [34]. Instead of feeding to the grid, the inverter is connected to the three phase load resistive loads as well. With specific design and type of the filter, nearly sinusoidal shape output waveforms can be achieved. This filter acts as a high impedance for higher order harmonics and low impedance for lower order frequency. It is recommended to set the cut-off frequency 1 or 2 octave above the fundamental frequency [35].

Simulation Model

A simulation in MATLAB/Simulink utilizing SimPowerSystem was conducted to investigate the effectiveness of the developed inverter control system. It was simulated for 0.16 seconds with a sampling period of 5 µs. The simulation modeling is shown in Fig. 5.

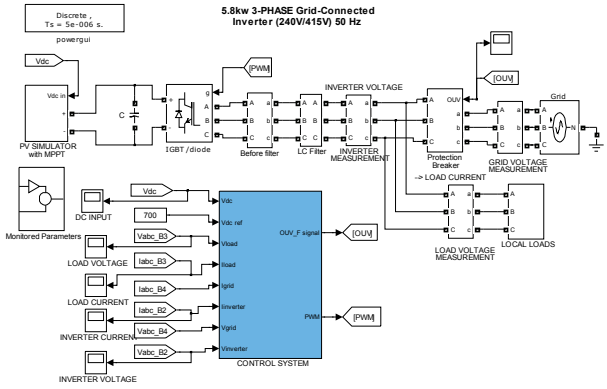

Fig. 5: Simulation model for PV three-phase grid-connected inverter

For evaluating the behavior of the inverter control algorithm especially the dynamic of the system power balance and the flow of power, the following load profiles are used:

(i) 5.8kW, where the generated power is the same as the absorption.
(ii) 3.0kW, where the load power requirement is less than that of the generator.
(iii) 8.8kW, where load power requirement is higher than that of the generator.

In addition, to assess the capability of the developed system protection, the disturbances in grid voltage and frequency are introduced. The disturbances are over voltage, under voltage, over frequency and under frequency. For grid-connected mode, the injected current must be nearly sinusoidal with a unity power factor and below 5% of total harmonic distortion (THD) [36].

Result and Discussion

In the following section, the simulation results are presented to validate the effectiveness of the developed inverter control system algorithm. Fig. 6 presents the three phase grid voltage waveforms, v_a, v_b and v_c in p.u.

As can be seen from the figure, during the initial period of 0.03s, the inverter operates in standalone mode to establish the grid synchronization. Obviously, the waveforms are almost sinusoidal and 120º displaced to each others. They exhibit a constant voltage of 1.0 p.u (240Vrms) with frequency of 50 Hz. The control algorithm is structured so that the inverter starts in off-grid (standalone) mode, operating as a voltage-controlled inverter, and then is synchronized with the grid at time t = 0.03s. Then from this time onwards, it operates in grid-connected mode, behaves as current-controlled inverter.

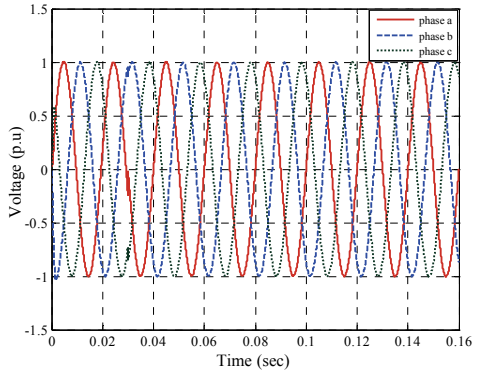

Fig. 6. Three phase grid voltages, v_a,v_b and v_c

Similarly, it can be seen that the current waveforms posses almost the same sinusoidal shape during the operation modes and this is shown in Fig. 7. Tiny ripples can be seen especially at the peak of the waveform during connecting to the grid, owing to the inverter current-controlled mode algorithm. This algorithm ensures that the injected current to the grid is maintained at a constant level.

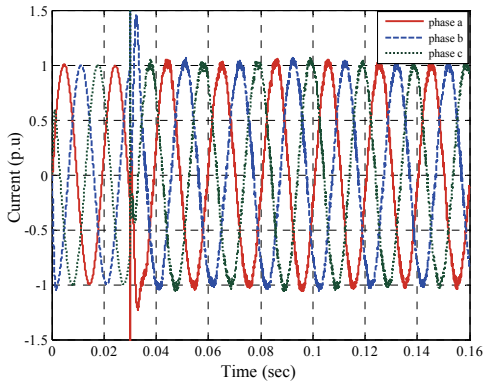

Fig. 7. Three phase Inverter output current waveforms, i_a, i_b and i_c

Fig. 8 illustrates the inverter dynamic flow of power with three different loads power demand in terms of grid power contribution.

As can be seen in the figure, during the off-grid mode, the 5.8kW power generated by the PV is transferred to the load of 5.8kW. This power balance condition between the generation and the absorption is continued until the early period of connection to the grid (0.03 to 0.05sec). As a result, there is almost no power being drawn from or dispatched to the grid as shown by the grid contribution profile.

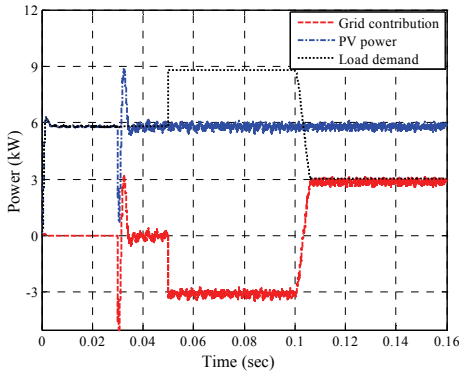

Fig. 8. Three phase inverter system power flow.

Then the load power is increased to 8.8kW (0.05 to 0.1 sec), which is equivalent to an increase of 3kW of power. Apparently, the additional power is drawn from the grid which was indicated by -3kW at the grid contribution profile. A scenario where the load demands less power from the PV is depicted in the period of 0.1 to 0.16 second. In other words, the load power is reduced to 3kW, causing the excess power of approximately 2.8kW being fed to the grid as can be seen in the grid contribution profile.

The above result of system power flow analysis implies the effectiveness of the control system algorithm in both standalone and grid interactive operation.

Fig. 9 and Fig. 10 show the THD of the phase voltage and current waveforms. They are 2.48% and 4.64% respectively, which are in compliance of below 5% of the IEEE standard. These results exhibit the effectiveness of the implementation of developed voltage and current-controlled algorithms, SPWM technique and filter as well.

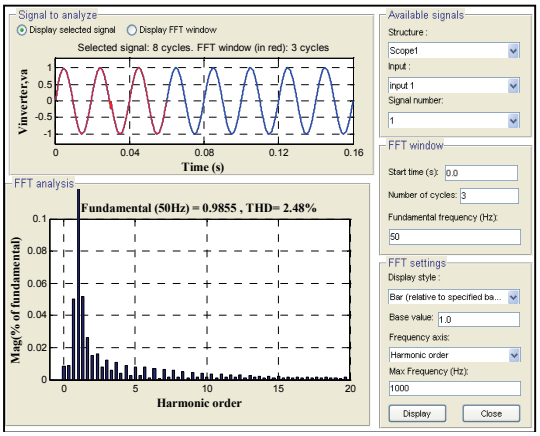

Fig.. 9. THD and harmonics spectrum of inverter output voltage

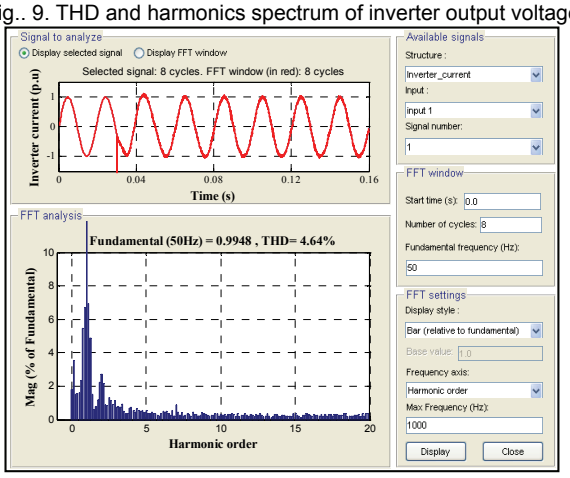

Fig. 10. THD and harmonics spectrum of inverter output current

The response of the developed inverter algorithm towards the grid disturbances are illustrated in the following figures. Fig. 11 shows the over-frequency disturbance scenario, where the grid frequency is increased to 51Hz. As mentioned previously, the inverter starts in off-grid mode, which is indicated in the figure by the zero grid current level, and then connects to the grid at 0.03 second. After detecting the disturbance which occurred from the period of 0.06 to 0.09 second, the inverter isolated itself from the grid, and then shut down at 0.113 second. The system disconnection period, which is the time of the disturbance occurrence to the time of grid disconnection, is approximately 2.65 cycles, which is in the compliance of the IEEE requirement. Obviously, it can be seen that after 0.113 second, the inverter voltage is zero and no current flowing to or from the grid, indicating the process of inverter shutting-down and grid-isolating phenomenon, as to provide safety protections for both device and personnel.

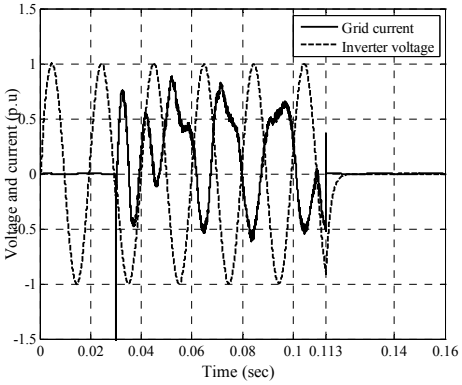

Fig. 11. Grid current and inverter voltage for grid frequency of 51Hz

The under-frequency situation of the grid frequency dropped to 49Hz is shown in Fig. 12. Initially, the inverter operates in off-grid mode, operating with zero grid current, and then connected to the grid at 0.03 second. It has detected the disturbance which occurred at 0.065 second, and then turned off and isolated itself from the grid at 0.118 second. Similar in the previous over-frequency situation, the inverter shutting down and isolating process took approximately 2.65 cycles which is within the range of the IEEE requirement. This can be seen from the figure after 0.118 second, whereby both the inverter voltage and grid current are zero, resulted from the occurrence of inverter shutting down and grid-isolating process.

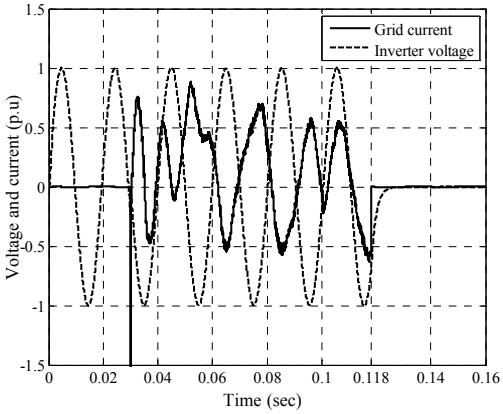

Fig. 12. Grid current and inverter voltage for grid frequency of 49Hz

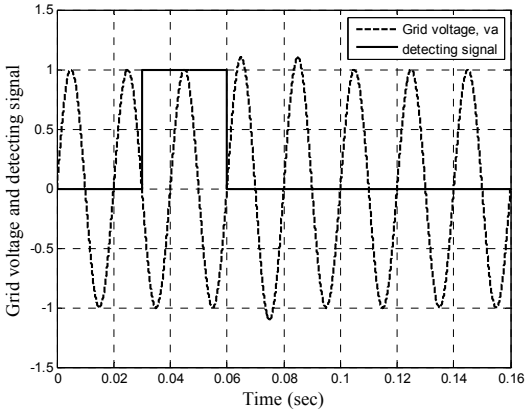

Fig. 13. Detecting signal for grid voltage of 264Vrms

Fig. 13 shows the inverter response in detecting grid voltage increase to 264Vrms. Firstly, the inverter operates in off-grid mode and then connects to the grid at 0.03 second, which shown by the 'high' voltage level of the detecting signal. The disturbance detection occurs at 0.06 second and caused the detecting signal to become 'low', disconnecting the system from the grid followed by the inverter switching-off. As a result, no grid current flowing through and the inverter terminal voltage became zero as illustrated in Fig. 14. The inverter behavior when the grid voltage dropped to 211Vrms is shown in Fig. 15. In the grid-connected mode, upon detection of the disturbance which occurs at 0.065, the control system generates the 'low' level detecting signal, isolating the inverter from the grid and at then switches itself off. As a result, there is no grid current flowing through, and the inverter terminal voltage become zero as illustrated in Fig. 16.

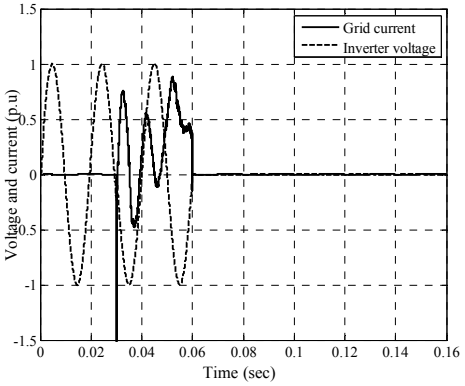

Fig. 14. Inverter voltage and grid current for grid voltage of 264Vrms

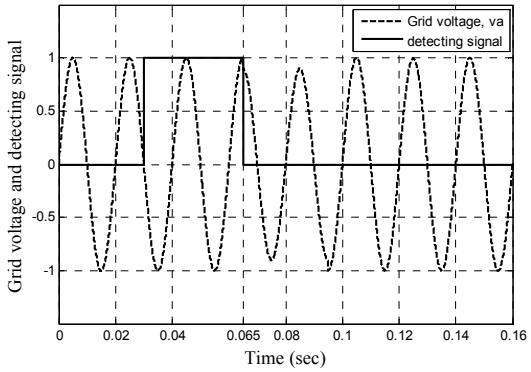

Fig. 15. Inverter voltage and grid current for grid voltage of 211Vrms

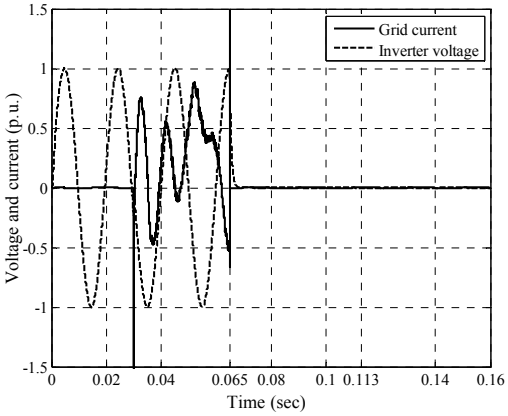

Fig. 16. Inverter voltage and grid current for grid voltage of 211Vrms

Table 1 presents the features of the proposed inverter in relation to the developed systems. As can be seen, the proposed inverter features are good compare to others especially in the waveform quality and hardware implementation.

Table 1. Comparison of proposed dSPACE inverter control scheme

Features	Ref.5	Ref. 12	Ref. 13	Ref. 22	Ref. 25	Proposed
Voltage THD	-	3.5%	-	6.8%	-	2.48%
Current THD	6.8%	-	19.8%	-	4%	4.64%
Power factor	-	-	unity	unity	-	unity
Topology	3Ø 3-level @transformer	3Ø 3-level	3Ø 3-level	1Ø 5-level	3Ø 3-level	3Ø 3level
Switching	PWM	PWM	SVPWM	SPWM	SVPWM	SPWM
Implement	simple	complex	complex	complex	simple	simple
Environment	programming	programming	programming	programming	prog/Simulink	Simulink

The waveform quality in terms of total harmonic distortion of the proposed model is 2.48% and 4.64% for voltage and current, respectively, which is better compare to some of the work as mentioned. The platform execution environment is simple compared to huge programming and computational burden. Moreover, this simulation would be linked to the PV inverter prototype development using dSPACE controller.

Conclusion

The investigation of the grid-connected three-phase inverter for the PV applications has been presented. The developed inverter control system modeling is carried out in MATLAB/SIMULINK environment with different load power demands and grid voltage and frequency disturbance scenarios. The presented results showed that the inverter control algorithm is successful in converting PV dc power to ac power with acceptable THD level for supplying power to the load and grid as well. In addition, the system manages to regulate the 50Hz sinusoidal output voltage and response to the grid voltage and frequency disturbances effectively. Overall, this investigation has proved the good performance of the developed inverter control system and protection algorithm.

REFERENCES

[1] Ahmad, G. E., Hussein, H. M. S., El-Ghetany, H. H., Theoretical Analysis and Experimental Verification of PV Modules, *Renewable Energy*, 28(2003), 1159–1168.

[2] Blaabjerg, F., Chen, Z., Kjaer, S., Power Electronics as Efficient Interface in Dispersed Power Generation Systems. *IEEE Trans. On Power Electronics*, 19(2004), no. 5, 1184-1194.

[3] Hassaine, L., Olias, E., Quintero, J., Haddadi, M., Digital Power Factor Control and Reactive Power Regulation for Grid-Connected Photovoltaic Inverter, *Renewable Energy*, 34(2009), no. 1, 315-321.

[4] Salas, V., Olias, E., Overview of State of Technique for PV Inverters Used in Low Voltage Grid-Connected PV Systems: Inverters Below 10kW, *Renewable and Sustainable Energy Rev.*, 13(2009), 1541-1550.

[5] Gounden, N. A., Peter, S. A., Nallandula H., Krithiga, S., Fuzzy Logic Controller with MPPT using Line-Communicated Inverter for Three-Phase Grid-Connected Photovoltaic Systems, *Renewable Energy*, (2009), no. 34, 909-915.

[6] Eltawil, M. A., Zhao, Z., Grid-connected Photovoltaic Power Systems: Technical and Potential problems-a review, *Renewable and Sustainable Energy Reviews*, 14(2010), no. 1, 112-129.

[7] Valentin O., Giovanni G., Filippo S., Dual Neutral-Point-Clamped Converters with Synchronized PWM for Photovoltaic Installations, *Int. Review of Electrical Engineering (IREE)*, 5(2010), no. 1, 56-63.

[8] Lima, J. C., Corleta, J. M., Medeiros, A., V. M. Canalli, Antunes, F., Libano, F. B, Dos Reis, F. S., A PIC Controller for Grid Connected PV System using a FPGA Based Inverter, *Proceeding of the IEEE Int. Symposium on Industrial Electronics (ISIE), 2000*, 169-173.

[9] Subiyanto, Mohamed, A., Hannan, M.A., Photovoltaic Maximum Power Point Tracking Controller Using a New High Performance Boost Converter, *Int. Rev. of Electr. Eng.* 5(2010), 6, 2535-2545.

[10] Hannan, M.A., Chan, K.W., Modern Power Systems Transients Studies Using Dynamic Phasor Models, Proceeding *of the International Conference on Power System Technology (POWERCON),* 2004, November, 21-24, Singapore.

[11] Hannan, M.A., Mohamed, A., PSCAD/EMTDC Simulation of Unified Series-Shunt Compensator for Power Quality Improvement, , *IEEE Transaction on Power Delivery*, 20 (2005), no. 2, 1650-1656.

[12] Hannan, M.A., Mohamed, A., Hussain, S., Al-Dabbagh, M., Power Quality Analysis of STATECOM Using Dynamic Phasor Modelling, *Int. J. of Electric Power System Res.*, 79(2008), no. 6, 993-999.

[13] Poh, C. L., Donald, G. H., Analysis of Multiloop Control Strategies for LC/CL/LCL-Filtered Voltage-Source and Current-Source Inverters, *IEEE Trans. on Industry Appl.*, 41(2005), no.2, 644-654.

[14] Buja, G. S., De Nardi, P., Application of a signal processor in PWM inverter control, *IEEE Trans. on Industrial Electronics*, 32(1985), no.1, 50-55.

[15] Alonso-Martinez, J., Eloy-Garcia, J., Arnaltes S, Direct Power Control of Grid-Connected PV Systems with Three Level NPC Inverter, *Solar Energy*, (2010), no. 84, 1175-1186.

[16] Mondzik, A., Baszyński, M., Piróg, S., Penczek., Szarek, A. M., Phase-Locked Loop for Grid-Connected Power Electronics Converters, *Przeglad Elektrotechniczny*, 02(2010), 335-

[17] Xiao-Qiang G., Wei-Yang W., He-Rong G., Phase locked loop and synchronization methods for gridinterfaced converters: a review, *Przeglad Elektrotechniczny*, 4 (2011), 182-187.

[18] Han, Y., Xu, L., Yao, G., Zhou L., Khan, M, Chen, C., Pan, J., M., Implementation of the PWM gating and IGBT protection scheme for the grid-connected multilevel inverter applications, *Przeglad Elektrotechniczny*, 7(2010), 360-365.

[19] Świeboda, P., Wawro, M., SVPWM algorithm in the scalar control structure for the three-phase voltage source inverter supplying two-phase high speed alternating current motors, *Przeglad Elektrotechniczny*, 10(2010), 311-316.

[20] Wang, H., Yue, X., Pei, X., Kang, Y., Voltage/current control mode for combined three-phase inverter, *Przeglad Elektrotechniczny*, 11a(2010), 358-364.

[21] Hannan, M.A., Ghani, Z.A., Mohamed, A., An Enhanced Inverter Controller for PV Appplications Using the dSPACE Platform, *International Journal of Photoenergy*, (2010), doi:10.1155/2010/457562, 1-10.

[22] Ghani, Z.A., Hannan, M.A., Mohamed, A., Renewable Energy Inverter Development using dSPACE DS1104 Controller Board. *Proceeding of the IEEE Conference on Power and Energy (PECon)*, (2010), 69-73.

[23] Salam, Z., Soon T. L., Ramli, M., Z., Hardware Implementation of the High Frequency Link Inverter Using dSPACE DS1104 Digital Signal Processing Board, *First International Power and Energy Conference (PECon)*, (2006), 348-352.

[24] Selvaraj, J., Nasrudin, A. R., Multilevel Inverter for Grid-Connected PV System Employing Digital PI Controller, *IEEE Transactions on Industrial Electronics,* 56(2009) no. 1, 149-158.

[25] Hmidet, A., Dhifaoui, R., Hasnaoui, O., Development, Implementation and Experimentation on a dSPACE DS1104 of a Direct Voltage Control Scheme, *Journal of Power Electronics*, 10(2010), no. 5, 468-476.

[26] Sera, D., Tamas Kerekes, Marian Lungeanu, Pezhman Nakhost, Remus Teodorescu, Gert K. Anderson, Marco Liserre, Low-Cost Digital Implementation of Proportional-Resonant Current Controllers for PV Inverter Applications using Delta Operator, *IEEE Industrial Electronics Society Conference (IECON)*, (2005), 2517-2522.

[27] Balouktsis, A., Karapantsios, T. D., Antoniadis, A., Balouktsis, I., Load Matching in a Direct-Coupled Photovoltaic System-Application to Thevenin's Equivalent Loads, *International Journal of Photoenergy*, (2006), 1-7.

[28] El Amrani, A., Mahrane, A., Moussa, F. Y., Boukennous, Y., Solar Module Fabrication, *Int. Journal of Photoenergy*, (2007), 1-5.

[29] Balouktsis, A., Karapantsios, T. D., Antoniadis, A., Paschaloudis, D., Bazergiannidou, A., Bilalis, N., Sizing Stand-Alone Photovoltaic Systems, *International Journal of Photoenergy*, (2006), 1-8.

[30] Perez, P. J., G. Almonacid, J. Aguilera, J. de la Casa, RMS Current of A Photovoltaic Generator in Grid-Connected PV Systems: Defination and Application, *Int. Journal of Photoenergy*, (2008), 1-8.

[31] Saadat, H., *Power System Analysis,* (McGraw-Hill Companies, Inc., 2004).

[32] Rahim, N. A, Selvaraj, J., Krismadinata, C., Five-level Inverter with Dual Reference Modulation Technique for Grid-Connected PV System. *Renewable Energy*, 35(2010), 712-720.

[33] Mohan, N., Underland, T. M, Robbins, W. P., *Power Electronics, Converters, Applications, and Design*, (John Wiley & Sons, Inc., 2003).

[34] Dai, M., Marwali, M. N., Jung, J. W., Keyhani, A., A Three-Phase Four-Wire Inverter Control Technique fo a Single Distributed Generation Unit in Island Mode, *IEEE Transactions on Power Electronics*, 23(2008), no. 1, 322-331

[35] Jacob, J. M., *Power Electronics: Principle & Applications*, (Delmar Thomson Learning Inc., 2002).

[36] IEEE Std 929-2000, *Recommended Practices for Utility Interface of Photovoltaic System*, (The Institute of Electrical and Electronics Engineers, New York, 2002).